JACS
JOURNAL OF THE AMERICAN CHEMICAL SOCIETY
Article
pubs.acs.org/JACS

Spectral Dependence of the Internal Quantum Efficiency of Organic Solar Cells: Effect of Charge Generation Pathways

Ardalan Armin,[†] Ivan Kassal,[‡] Paul E. Shaw,[†] Mike Hambsch,[†] Martin Stolterfoht,[†] Dani M. Lyons,[†] Jun Li,[§] Zugui Shi,[§] Paul L. Burn,*[,†] and Paul Meredith*[,†]

[†]Centre for Organic Photonics & Electronics (COPE), School of Mathematics and Physics, and School of Chemistry and Molecular Biosciences, The University of Queensland, Brisbane 4072, Australia

[‡]Centre for Engineered Quantum Systems, Centre for Quantum Computation and Communication Technology, and School of Mathematics and Physics, The University of Queensland, Brisbane 4072, Australia

[§]Institute of Materials Research and Engineering, Agency for Science, Technology and Research, Singapore 117602

Supporting Information

ABSTRACT: The conventional picture of photocurrent generation in organic solar cells involves photoexcitation of the electron donor, followed by electron transfer to the acceptor via an interfacial charge-transfer state (Channel I). It has been shown that the mirror-image process of acceptor photoexcitation leading to hole transfer to the donor is also an efficient means to generate photocurrent (Channel II). The donor and acceptor components may have overlapping or distinct absorption characteristics. Hence, different excitation wavelengths may preferentially activate one channel or the other, or indeed both. As such, the internal quantum efficiency (IQE) of the solar cell may likewise depend on the excitation wavelength. We show that several model high-efficiency organic solar cell blends, notably PCDTBT:PC70BM and PCPDTBT:PC60/70BM, exhibit flat IQEs across the visible spectrum, suggesting that charge generation is occurring either via a dominant single channel or via both channels but with comparable efficiencies. In contrast, blends of the narrow optical gap copolymer DPP-DTT with PC70BM show two distinct spectrally flat regions in their IQEs, consistent with the two channels operating at different efficiencies. The observed energy dependence of the IQE can be successfully modeled as two parallel photodiodes, each with its own energetics and exciton dynamics but both having the same extraction efficiency. Hence, an excitation-energy dependence of the IQE in this case can be explained as the interplay between two photocurrent-generating channels, without recourse to hot excitons or other exotic processes.

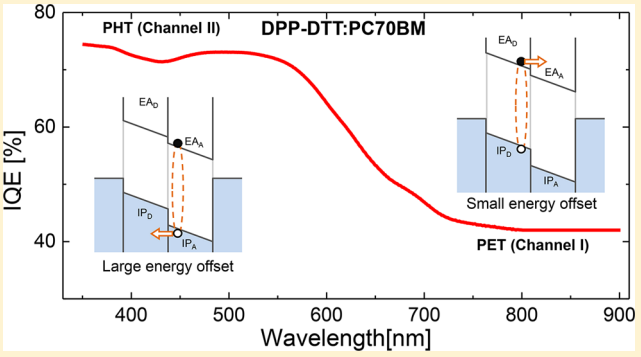

INTRODUCTION

The junction of an organic solar cell is made from combinations of organic semiconductors sandwiched between appropriate transport layers and electrodes. In direct analogy to their doped inorganic counterparts which consist of n- and p-doped components,[1] organic solar cell junctions consist of two materials: an electron acceptor and an electron donor in intimate contact at the molecular level. The acceptors and donors have different ionization potentials and electron affinities, and the differences in these between the materials rather than their absolute values are critical to charge generation.[2,3] Photoexcitations in organic semiconductors are excitonic in nature, and hence the resultant electron−hole pairs experience strong Coulomb binding because of the low dielectric constants and the spatial localization of electron and hole wave functions.[4] The resulting binding energies are around 0.5 eV.[5] Thermal fluctuations at operational temperatures or moderate external electric fields ($<10^4$ V/cm)[6] do not provide sufficient energy to separate the electrons from the holes. Although the precise mechanism of free carrier generation in organic solar cells is still not completely understood, it is generally accepted that the acceptor−donor molecular heterojunction does provide sufficient energy to effectively split an exciton. It is also accepted that the exciton-to-free-carrier transition occurs primarily via an intermediate charge-transfer (CT) state where the electron−hole pair remains weakly bound (and spin correlated[7]) but resides on two different (macro)molecules. The precise details (e.g., rates) of the energetics and dynamics of the interface and the CT state are dependent upon a number of complex factors, including the energy levels in the acceptor and donor, the exciton binding energy, the local disorder at phase boundaries, and the domain structure.[8]

Exciton dissociation in standard high-efficiency organic solar cells is commonly described to occur via photoexcited electron

Received: May 30, 2014
Published: August 4, 2014

   dx.doi.org/10.1021/ja505330x | J. Am. Chem. Soc. 2014, 136, 11465−11472

transfer (PET) from the donor to the acceptor.[9−11] In this scenario the donor component absorbs the solar radiation, and the resulting exciton quickly relaxes to the lowest-lying singlet excited state due to strong vibronic coupling.[12−14] The excited electron is then transferred to the acceptor (Figure 1a,c).

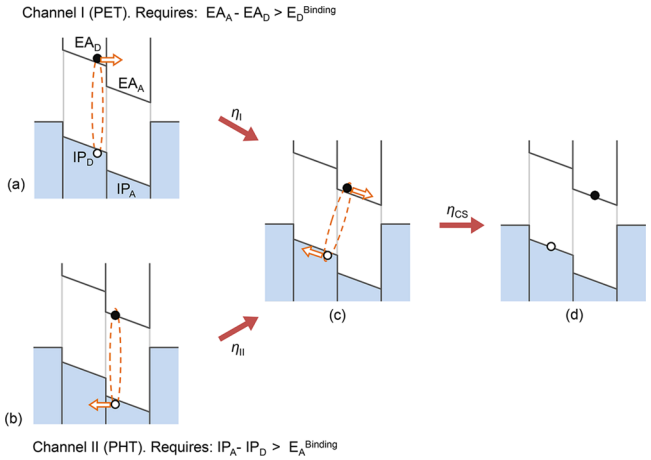

Figure 1. (a) and (c): Photoexcited electron transfer. (a) Simplified energy diagram of a donor−acceptor interface with different electron affinities [EA, often equated to the lowest unoccupied molecular orbital (LUMO) energy] and ionization potentials [IP, often equated to the highest occupied molecular orbital (HOMO) energy]. The electrodes (outer rectangles) are shown at short circuit. After photoexcitation in the donor, the exciton (with Coulomb binding energy $E_D^{binding}$) diffuses to an acceptor−donor interface, after which an electron can transfer into the acceptor LUMO with efficiency η_I (orange arrow). (b) and (c): Photoexcited hole transfer. (b) An exciton (with Coulomb binding energy $E_A^{binding}$) in the acceptor dissociates at the interface with efficiency η_{II}. [Remark: If both phases absorb light, both PET and PHT can simultaneously contribute to charge generation, provided both of the energy conditions hold.] (c) and (d): The resulting relaxed interfacial CT state dissociates to free polarons with efficiency η_{CS}.

However, it has been established that photoexcitations on the acceptor can also significantly contribute to the photocurrent through photoexcited hole transfer (PHT) to the donor.[15−19] In this case a ground-state electron is transferred from the donor to the excited acceptor (Figure 1b,c). The PHT efficiency will depend on the energy offset between the oxidation potential of the donor and the reduction potential of the excited acceptor. PET and PHT have also been termed Channel I and Channel II, respectively, as a matter of convenient nomenclature.[18,20] In principle, the two channels are thermodynamically equivalent from the point at which the CT state is formed and thermally relaxes. Dissociation of the CT state then leads to the free charge carriers (Figure 1c,d). Appreciation of the fact that both acceptor and donor absorption can contribute directly to photocurrent generation has led to the concept of complementary absorption, enabling higher power conversion efficiencies than would be obtained with Channel I only.[21]

In spectral regions where the donor and the acceptor both absorb, Channels I and II can operate simultaneously[18] as two parallel photodiodes (photocurrent addition). However, the simultaneous operation of the two channels makes it difficult to disentangle their individual contributions and determine the factors that govern their relative efficiencies. Clearly, the contribution of each channel will be primarily dependent on the contribution to the optical density of the active layer by each component, which will be dependent on the extinction coefficient of each component and the relative concentration ratio of the materials. Furthermore, factors such as the alignment of energy levels, differences in exciton binding energies (caused by differences in dielectric constants or delocalization lengths between the donor and acceptor), exciton diffusion lengths, or the rates of charge transfer, which in turn depend on parameters such as the reorganization energies and the quantum-mechanical transfer integrals in Marcus−Hush theory, can also affect the efficiency of each channel.[8] If the two channels are not equally efficient, the overall internal quantum efficiency (IQE) may be energy-dependent, being higher at those wavelengths that preferentially excite the more efficient channel. Conversely, if the donor and acceptor absorption spectra differ, and yet the device has a spectrally flat IQE, we can conclude that Channels I and II are equally efficient at generating free carriers.

Recently, the concept of hot excitons has been advanced as a means to explain increased exciton dissociation efficiency in organic solar cells by excess photon energy.[22−25] The hot exciton process should produce an energy-dependent IQE behavior (the more energetic photons creating more free carrier pairs), and whether this occurs remains a controversial topic.[26,27] However, because differing Channel I and Channel II efficiencies can likewise generate energy-dependent IQEs, one must fully understand the photocurrent-generating pathways before invoking this more exotic behavior.

In this article, we describe three high-efficiency organic solar cell acceptor−donor combinations that have equal Channel I and Channel II efficiencies, and one new system that has a marked energy dependence of the IQE. We demonstrate clearly that this energy dependence is due to unequal Channel I and Channel II efficiencies (not the excess energy of hot excitons), and we model the situation with a simple two-photodiode description.

RESULTS AND DISCUSSION

We begin with the donor−acceptor combination poly[*N*-9″-heptadecanyl-2,7-carbazole-*alt*-5,5-(4,7-di-2-thienyl-2,1,3-benzothiadiazole)]:[6,6]-phenyl-C71-butyric acid methyl ester (PCDTBT:PC70BM), which demonstrates power conversion efficiencies (PCEs) in excess of 6%[28,29] with high fullerene loadings (80% by weight PC70BM, or a 1:4 ratio by weight). In Figure 2a, we present the solid-state absorption of PCDTBT, PC70BM (weighted on the basis of volume ratio to match the blend absorption), and the 1:4 blend as thin films on quartz (as calculated from the measured transmittance) as well as the absorption of equivalent full devices (ITO/PEDOT:PSS/junction/Al with an 80 nm junction thickness, see the Experimental Section) derived from near-normal-incidence reflectance measurements. Notably, the absorption spectra of PC70BM and the 1:4 blend thin films are similar. The similarity is even more striking in the corresponding full devices and points to an insignificant contribution of PCDTBT to the light absorption of the blend, which is consistent with its extinction coefficient and the fact that it is only 20 wt% of the film.

On the basis of these optical measurements, one would assert that the majority of photocurrent is generated by fullerene absorption. This is confirmed by the data in Figure 2b, which show external quantum efficiency (EQE) measurements for equivalent devices containing an optimized 1:4 (20 wt% PCDTBT) junction and one containing only 5 wt% polymer,

dx.doi.org/10.1021/ja505330x | J. Am. Chem. Soc. 2014, 136, 11465−11472

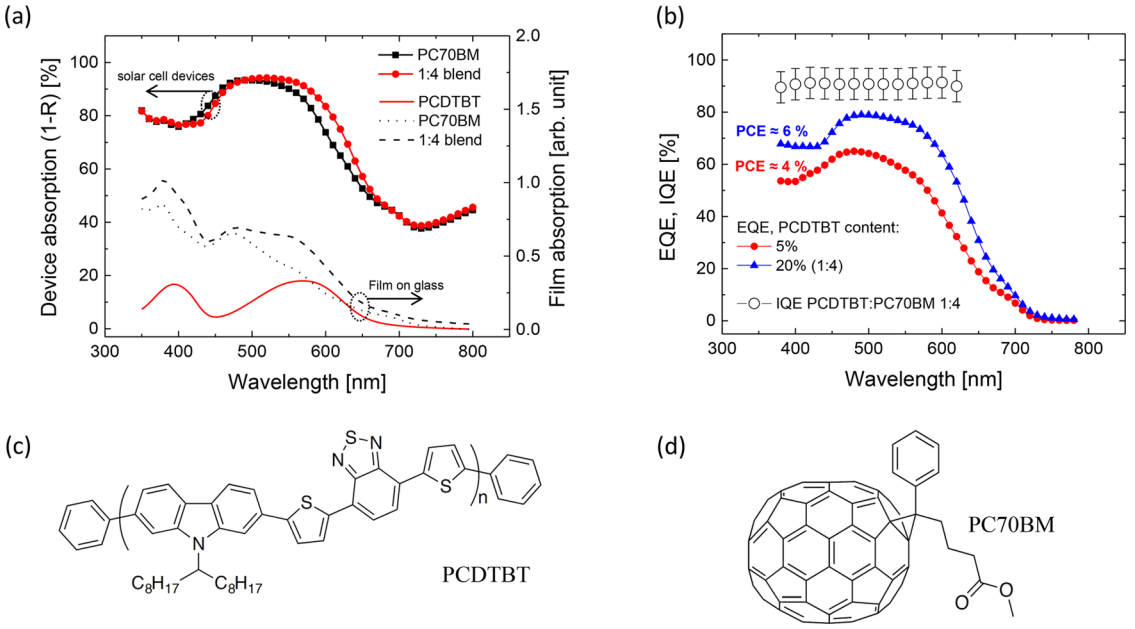

Figure 2. (a) Thin film optical absorption of PCDTBT, PC70BM, and a 1:4 (by weight) blend on quartz (as calculated from the measured transmittance) and of equivalent organic solar cells with 80 nm junction thickness derived from near-normal-incidence reflection measurements. PCDTBT and PC70BM absorptions are weighted on the basis of their volume ratio. The total absorption spectra of the 1:4 blend and PC70BM-only solar cells are very similar, indicating that PC70BM is dominantly responsible for light film absorption in the 1:4 blend. (b) External quantum efficiencies (EQEs) of PCDTBT:PC70BM solar cells with PCDTBT content of 20% and 5% (also 80 nm junction thickness). The power conversion efficiencies (PCEs) of each device, measured at AM1.5G and 100 mW/cm^2, are indicated. These devices are typical of the 12 cells fabricated. The internal quantum efficiency (IQE) is also shown for a typical PCDTBT:PC70BM 1:4 device, and it does not possess significant spectral dependence within the uncertainty of the measurement (shown as the error bars and derived from a chain rule analysis of all experimental parameters as described in the SI). (c,d) Molecular structures of PCDTBT and PC70BM.

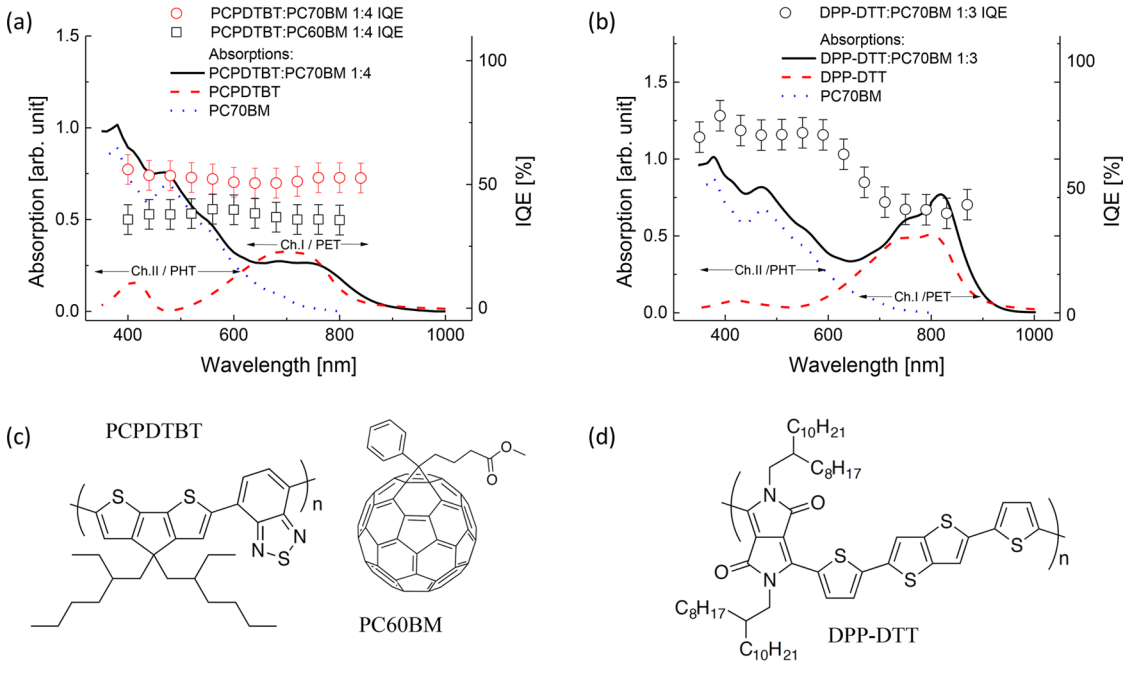

Figure 3. (a) Absorption spectra of PCPDTBT, PC70BM, and their 1:4 (by weight) blend. The internal quantum efficiency (IQE) spectra for PCPDTBT:PC70BM and PCPDTBT:PC60BM organic solar cells are also shown, derived again from the whole of device reflectance measurements and transfer matrix calculations. For these two cases, the IQE is spectrally flat within the experimental uncertainty (~6% as described in the SI). (b) Absorption spectra of PC70BM, DPP-DTT, and their 1:3 (by weight) blend, showing the separation of the component absorptions and therefore indicating that the two photocurrent channels can be disentangled. The IQE for DPP-DTT:PC70BM solar cells is also shown. In contrast to the spectrally flat IQE of PCPDCTBT:PC60/70BM, DPP-DTT:PC70BM exhibits a two-step IQE corresponding to Channels I and II operating at different efficiencies. The absorption spectra of neat materials are weighted on the basis of their volume ratio in the blend. (c,d) Molecular structures of PCPDBT, PC60BM, and DPP-DTT.

dx.doi.org/10.1021/ja505330x | J. Am. Chem. Soc. 2014, 136, 11465−11472

both of the same thickness (~80 nm) to negate significant optical cavity effects [see the Supporting Information (SI), Figure S1, for current density−voltage curves]. The shapes of the EQEs are very similar, and the 5 wt% polymer solar cell produces only a slightly lower PCE of 4%. This is in agreement with a recent report on optically pumped PCDTBT:PC70BM transistors, suggesting that 80−90% of the photocurrent generation is produced in the fullerene.[30] The PCE differences in the 5 wt% polymer blend versus the fully optimized 1:4 blend arise due to relative differences in hole-extraction efficiency[29] and potentially a deficit in acceptor−donor interfaces for exciton dissociation.

Next we determined the IQE of the PCDTBT:PC70BM 1:4 blend. It is important to note that the full device reflectance measurements in combination with transfer matrix simulations, which account for parasitic absorptions in the nonactive layers[31] and light scattering,[32] must be used to accurately calculate the IQE[17,31,32] (more details are provided in the SI, Figure S2). In this analysis we assumed that the charge collection efficiencies at the electrodes were independent of the energy of the incoming photons,[23,33] meaning that the spectral shape of the IQE should be related to the spectral shape of the charge generation efficiency. We will return to this assumption later in this article. Figure 2b shows the IQE determined for a 1:4 PCDTBT:PC70BM solar cell. In agreement with our previous report,[31] it was found that the IQE is spectrally flat; i.e., the charge generation yield does not depend on the photon energy. Due to substantial spectral overlap between donor and acceptor in these solar cells, one cannot immediately conclude that both photocurrent channels have the same efficiencies; however, because it has been shown that the PCDTBT:PC70BM device is predominantly Channel II, this question has no impact.

We then examined three systems containing narrow optical gap donors and fullerene acceptors with identifiable spectral regions where one of the phases is the dominant absorber, and in which we can expect substantial contributions from both photocurrent-generating pathways. These systems were poly-[2,6-(4,4-bis-{2-ethylhexyl}-4*H*-cyclopenta[2,1-*b*;3,4-*b*′]-dithiophene)-*alt*-4,7-(2,1,3-benzothiadiazole):[6,6]-phenyl-C61-butyric acid methyl ester (PCPDTBT:PC60BM) (1:4 by weight), PCPDTBT:PC70BM (1:4 by weight), and poly(*N*-alkyldiketopyrrolopyrrole dithienylthieno[3,2-*b*]thiophene) (DPP-DTT):PC70BM (1:3 by weight). PC60BM has a weaker absorption compared to PC70BM at longer wavelengths and hence provides a method for tuning the polymer absorption contribution.

Figure 3a shows the absorption spectra of PCPDTBT, PC70BM (weighted on the basis of volume ratio), and their 1:4 blend as well as the IQEs for solar cells made from PCPDTBT:PC70/60BM. The absorption spectrum of the PCPDTBT:PC70BM blend at wavelengths shorter than 600 nm is dominated by PC70BM and at longer wavelengths by PCPDTBT, as can be seen from the individual absorptions, and more so in the case of PC60BM. This is a clear situation where we can spectrally disentangle Channels I and II. The IQEs are again determined from whole-cell reflectance measurements in combination with transfer matrix calculations and EQE spectral responses.[27,31] In agreement with previous studies on different PCPDTBT:PC70BM blends,[26,27,31,34] our measured IQEs are spectrally flat within experimental uncertainty for both PC70BM and PC60BM (as described in the SI). Again, assuming that the carrier extraction efficiencies at the electrodes are energy-independent, this indicates that Channels I and II operate with efficiencies that are equal within experimental uncertainty. The fact that the IQEs are flat for different reported blend ratios and with both PC60BM and PC70BM indicates that the equivalence of the two channels is unlikely to be coincidental.

As in the PCPDTBT case, we show the relevant absorption spectra (weighted on the basis of volume ratio) in Figure 3b for DPP-DTT and its blend with PC70BM (1:3). This ratio has previously been identified as the optimum on the basis of detailed morphological and processing studies for a very similar DPP-based polymer:PC70BM system.[35] Again, the difference in absorption spectra enable the two photocurrent generation channels to dominate at different wavelengths. However, unlike the PCPDTBT case, the IQE of the DPP-DTT:PC70BM blend (1:3) shows a strong energy dependence. Between 400 and 600 nm, the spectral response is relatively flat. In this region the device is predominantly operating via Channel II because the polymer does not have significant absorption (Figure 3b). At wavelengths longer than 700 nm, the IQE is also flat, and in this region the device is operating predominantly via Channel I, where the polymer absorption dominates that of the fullerene. The transition between the two regimes occurs between 600 and 700 nm. This behavior can be simply modeled by considering the cell as two parallel photodiodes, with Channel I having IQE_I = 42% and Channel II having IQE_{II} = 77% (see Figure 4). The total IQE is then given by

$$IQE(\lambda) = \frac{x_D\alpha_D(\lambda)IQE_I + x_A\alpha_A(\lambda)IQE_{II}}{x_D\alpha_D(\lambda) + x_A\alpha_A(\lambda)} \quad (1)$$

where x_D is the volume fraction of the donor phase and $\alpha_D(\lambda)$ is the absorbance of the pure donor at wavelength λ (and likewise for the acceptor). Figure 4 shows the calculation of the IQE using the estimated volume fraction x_D = 0.3, assuming a mass density of 1.1−1.2 g/cm^3 for the polymer[36,37] and 1.6 g/cm^3 for PC70BM.[37]

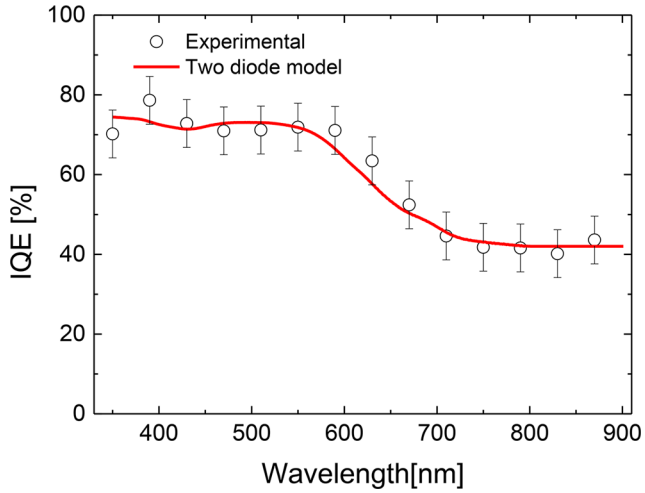

Figure 4. IQE of the DPP-DTT:PC70BM (1:3) system, measured and modeled as two photodiodes in parallel using eq 1.

Although an energy-dependent IQE could indicate that the excess energy of hot excitons enhances charge generation efficiency, that is not the case here. The fact that the IQE is flat within experimental error at wavelengths both below 600 nm and above 700 nm is strong evidence that both Channel I and Channel II efficiencies are independent of photon energy. The

dx.doi.org/10.1021/ja505330x | J. Am. Chem. Soc. 2014, 136, 11465−11472

energy dependence of the IQE between 600 and 700 nm is simply caused by the transition between the two dominant single-channel regions where both acceptor and donor absorptions are contributing photocurrent. This underscores the fact that the energy dependence of the IQE in a narrow part of the spectrum[33] may be misleading, insofar as it obscures the possibility that the IQE may be flat in other parts of the spectrum.

To gain some insight into why the efficiencies of the two channels are equal in PCPDTBT:PC70BM but different in DPP-DTT:PC70BM, we considered the energy levels of the materials (Figure 5). It should be noted that such diagrams can only be at best a guide due to the different errors associated with the various experimental techniques and the fact that the properties of the bulk material may not accurately reflect the local energetics at an interface due to disorder or local dipole effects. For example, typical values of energetic disorder in organic semiconducting polymers are on the order of 100 meV or more.[8] The ionization potentials in Figure 5 were measured by photoelectron spectroscopy in air (PESA) on neat films of the materials. It is generally agreed that PESA gives an accurate measure of the ionization potential. While experimental methods exist for the determination of the ionization potential and hence whether Channel II can or cannot occur, the same cannot be said for Channel I. The problem is that there is not a reliable way to determine the electron affinities of the materials. While inverse photoelectron spectroscopy has been used, materials that have a high proportion of protons lead to large errors in the measured electron affinity. Furthermore, electron affinities determined using electrochemical methods and/or optical spectroscopy are strongly dependent on the analysis method used (e.g., onset of reduction versus $E_{1/2}$ and onset versus peak absorption, respectively). We have previously used the crossover between the absorption and photoluminescence spectra corrected in energy[38] as an established method to determine the optical gap.[39] However, DPP-DTT is not luminescent, and so to be consistent across all three polymers, we have estimated the LUMO energy to be the onset of the film absorption (see SI, Figure S3). It should be noted that the optical gaps determined from the crossover of the PL and absorption spectra and those from the absorption onset (Figure S3) were similar and hence provide a level of confidence for the evaluation of the electron affinities and analysis.

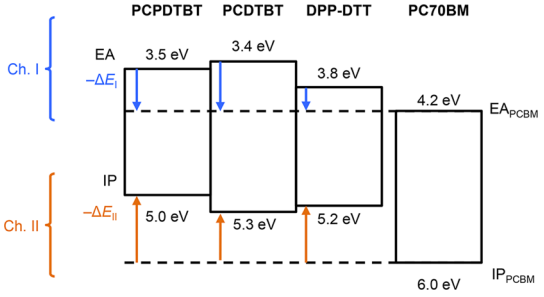

Figure 5. Energy levels for the donor–acceptor systems used in this paper. The IP values were determined by photoelectron spectroscopy in air, and the spectroscopically measured optical gaps were used to determine the EAs. Crucially, all donor–acceptor combinations have a large energetic driving force except for Channel I in DPP-DTT:PC70BM, which, we argue, is the origin of the two-step IQE in that blend.

On the basis of our approach, it would be expected that charge generation by the Channel II mechanism should be efficient for all the polymers due to the fact that the energy offset is between 0.7 and 1.0 eV (Figure 5), which is significantly larger than the exciton binding energy in many conjugated polymers. From our analysis based on PESA and the optical gap, we found that, in PCPDTBT and PCDTBT, the LUMO energies (electron affinities) were essentially the same. Furthermore, the electron affinities of these two polymers were less than that of DPP-DTT. That is, the electron affinity of DPP-DTT was closer to that of PC70BM. Clearly in the case of PCPDTBT and PCDTBT, the energy offsets between the polymer and fullerene are sufficient for efficient Channel I charge generation independent of disorder and the local environment. In the case of DPP-DTT the situation is not as clear-cut due to the fact that the energy levels are closer. The small energy offset may be insufficient for dissociation of photoexcitations such as excitons (Marcus–Hush theory) or CT states (as shown by Ohkita et al.[40]). The fact that some charge is still generated means that at least a portion of the polymer chains have a suitable LUMO energy to enable oxidation of the exciton (PET), but not all. That is, disorder and variations in the local environment can lead to a distribution in donor LUMO energies such that PET is energetically favorable only in certain parts of the blend and not others. This is in contrast to cases with large LUMO offsets, where the donor LUMO is above the acceptor LUMO regardless of local disorder. However, we cannot rule out the effect of morphological factors on the efficiencies of the two channels caused by differences in the exciton diffusion lengths relative to the domain size for both DPP-DTT and PC70BM.

Finally, we return to the relationship of the IQE spectral shape to the charge generation quantum yields. Since the IQE spectral shape could also be attributed to an energy-dependent charge collection efficiency, we will first consider this possibility. Charge collection efficiency is commonly considered to be independent of the incident photon energy when the spectral shape of the IQE is directly related to charge generation quantum yield.[23,33] However, there is some debate as to whether this assumption is valid in all circumstances. If the assumption does hold, one can directly relate any spectral features or dependencies in the IQE to charge generation, as we have done here. One also needs to consider that, when the charge carrier mobility is independent of the incident photon energy, the photogenerated carrier profile still depends on the incident light wavelength (energy)[41] due to optical cavity effects. For thin, high-efficiency devices, one can assume an efficient charge collection for electrons and holes regardless of the generation distribution profile. However, this assumption is not valid for thick junctions, where the drift distance of the charge carriers will be strongly dependent on the wavelength (see SI, Figure S4), and indeed the photogeneration profile may be in the Beer–Lambert regime (exponentially decaying optical field as a function of penetration distance in the cavity). Despite using relatively thin devices in this work, we confirmed using photoinduced absorption (PIA) spectroscopy that the IQE spectral dependence was directly related to the carrier generation efficiency, at least in DPP-DTT:PC70BM blends with a junction thickness of 140 nm.

PIA spectroscopy was performed on DPP-DTT:PC70BM films at three different excitation wavelengths: 445, 650, and 808 nm. These wavelengths were chosen because they predominantly photoexcited Channel I (808 nm), Channel II

dx.doi.org/10.1021/ja505330x | J. Am. Chem. Soc. 2014, 136, 11465–11472

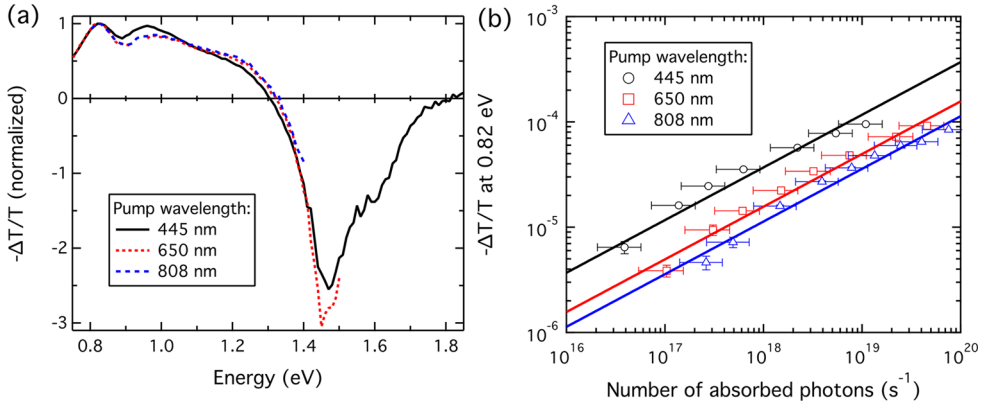

Figure 6. (a) Photoinduced absorption spectra of DPP-DTT:PC70BM blends obtained with pump wavelengths of 445, 650, and 808 nm and normalized relative to the peak at 0.82 eV. (b) Power dependence of the photoinduced absorption signal at 0.82 eV for each pump wavelength relative to the number of photons absorbed by the blend. Fits to the data with power = 0.5 are included as solid lines.

(445 nm), or both (650 nm), enabling us to probe the relative charge-carrier generation efficiencies. The normalized PIA spectra measured with each pump wavelength are shown in Figure 6a, and it can be seen that they have essentially the same shape with peaks at ∼0.82 and ∼0.98 eV, although the relative intensities of the features are a little different. A previous investigation into the polaron absorption of DPP-DTT identified peaks at 0.89 and 1.36 eV and a shoulder at 1.1 eV, which were assigned to intrachain polarons, cofacial interchain polarons, and staggered interchain polarons, respectively.[42] The peak at 1.36 eV is not present in our data, and the other features appear to have shifted to lower energies. However, we found that the presence or absence of the peak was processing solvent dependent, and hence we attributed this behavior to differences in the microstructure of the film. Nonetheless, the spectra provide strong evidence that there is no significant difference in the resulting distribution of polaronic states from photoexciting via Channel I or II. The power dependence of the PIA signal at 0.82 eV for each pump wavelength is displayed in Figure 6b and shows that the relative yield of long-lived polarons when exciting at 650 and 808 nm, and therefore invoking predominantly Channel I, is lower than when exciting at 445 nm. This effect is consistent with the IQE measurements and a difference between Channel I and Channel II charge-carrier generation. A good fit with power = 0.5 on these data confirms the dominance of bimolecular recombination of the carriers under open-circuit conditions, where all generated carriers eventually undergo recombination. Overall, the PIA data strongly support the assertion that the IQE spectral dependence we observe in the DPP-DTT system is due to charge generation, not collection.

CONCLUSIONS

Polymer:fullerene donor−acceptor blends in organic solar cells can generate photocurrent via two channels, driven by absorption in the relevant components and giving rise to either photoinduced electron transfer or photoinduced hole transfer (PET and PHT, Channel I and Channel II, respectively). In this article we present a study of the relevant efficiencies of these two channels in a number of high-efficiency bulk heterojunction systems. In three cases—PCDTBT:PC70BM, PCPDTBT:PC60BM, and PCPDTBT:PC70BM—the channels have experimentally indistinguishable efficiencies, and this produces a spectrally flat IQE. In the DPP-DTT:PC70BM system there is a marked "step" in the IQE, attributed to different Channel I and Channel II charge-generation efficiencies and driven by the markedly different energetics of PET and PHT for the materials studied. The spectral dependence of the IQE in this system can be explained using a two-channel model without recourse to more exotic phenomena such as hot excitons. Once again, it is important to note that accurate assessment of the IQE using whole-device reflectance measurements in combination with transfer matrix simulations is essential to gain mechanistic insight into the charge generation and collection processes in thin-film solar cells. Our results also demonstrate the importance of optimizing the energetics of both PET and PHT in order to fully exploit the concept of a dual-channel, complementary-absorber single junction.

EXPERIMENTAL SECTION

Materials and Solutions. PCDTBT ($\overline{M}_w$ = 122 kDa, PDI = 5.4) was purchased from SJPC, Canada. Molecular weights of PCDTBT were determined with gel permeation chromatography (GPC) in 1,2,4-trichlorobenzene at 135 °C by SJPC, Canada. PCPDTBT was synthesized and purified in-house as described previously[43] ($\overline{M}_w$ = 14 kDa and PDI = 1.3). DPP-DTT ($\overline{M}_w$ = 350 kDa and PDI = 2.8) was synthesized on the basis of the methodology described in detail in ref 44. Fullerenes were purchased from ADS. DPP-DTT was dissolved in chlorobenzene (CB) containing 7% 1,2-dichlorobenzene (DCB) at 120 °C, slowly cooled to 70 °C, and mixed with a solution of PC70BM in the same solvent blend. The solution was then slowly cooled to room temperature and filtered through glass wool. PCDTBT was dissolved in DCB at 150 °C, slowly cooled to 70 °C, and mixed with PC70BM solution. The solution was then cooled to room temperature and filtered through glass wool. PCPDTBT was dissolved in DCB at ambient temperature, mixed with PC70/60BM solution in DCB, and filtered through a 0.45 micron PTFE filter. The total concentrations of the solutions were as follow: PCDTBT:PC70BM, 25 mg/mL; DPP-DTT:PC70BM, 6 mg/mL; PCPDTBT:PC70BM, 40 mg/mL; and PCPDTBT:PC60BM, 40 mg/mL.

Solar Cell Device Fabrication. First, 15 Ω/sq. indium tin oxide-coated glass substrates (Xinyan) patterned by photolithography were precleaned using Alconox (detergent) solution and a soft cloth before being sonicated in sequence with Alconox, deionized water, acetone, and 2-propanol for 10 min each. Each substrate was 2.5 cm × 2.5 cm, with 6 pixels each 0.2 cm^2. The cleaned substrates were coated with a 25 ± 5 nm layer of poly(3,4-ethylenedioxythiophene):poly(styrenesulfonate) (PEDOT:PSS), purchased from Heraeus, by spin-coating at 5000 rpm for 60 s. The PEDOT:PSS layer was baked for 10 min at 170 °C. To obtain an 80 nm thick PCDTBT:PC70BM layer, the blend solution was spin-coated at 1500 rpm. PCPDTBT:PC60BM (1:4) and PCPDTBT:PC70BM (1:4) solutions with total concentration of 40

dx.doi.org/10.1021/ja505330x | J. Am. Chem. Soc. 2014, 136, 11465−11472

mg/mL were spin-coated at 600 and 1600 rpm, respectively. A blend solution of DPP-DTT:PC70BM (1:3) at a total concentration of 8 mg/mL was spin-coated at 500 rpm. The films were visually monitored during the spin coating, and the spin coater was turned off when the Newton fringes disappeared, i.e., the film had dried. The fabrication was carried out in a nitrogen atmosphere (O_2 <1 ppm, H_2O <1 ppm) at ∼20 °C. The thicknesses of the junctions were measured by a Veeco Dektak 150 profilometer. Finally, the devices were completed by depositing 1 nm of samarium and 100 nm of aluminum by thermal evaporation under a 10^{-6} mbar vacuum.

Photovoltaic Device Characterization. Current-density−voltage (J−V) characteristics were acquired in a nitrogen atmosphere using a Keithley 2400 source measure unit under simulated air mass 1.5 global (AM 1.5 G) 1000 W/m^2 illumination (as determined by an NREL-calibrated photodiode) provided by an Abet Sun 2000 solar simulator. EQEs were measured with a QEX7 setup from PV Measurements Inc., using an integrating sphere and calibrated photodiode. The total reflection spectra of the solar cells were determined at an incident light angle of <10°. The parasitic absorptions in nonactive layers were simulated using a computer code developed by van de Lagemaat et al. based on the transfer matrix method presented by Pettersson et al.[45] The IQE was determined by dividing the EQE by the net absorption within the active layer (junction).[31] Six devices were tested for each case. The variations in EQE were less than 5% as a result of precisely controlling the thickness uniformity, and the integrated EQEs were within ±10% of short-circuit current. This methodology fully accounts for cavity effects in thin-film solar cells and returns an accurate IQE.

Photoelectron Spectroscopy in Air (PESA). PESA measurements were performed using a Riken Kekei AC-2 spectrometer. For all samples a power intensity of 5 nW was used. The data were fitted as the square root of the electron count versus energy.

Photoinduced Absorption (PIA) Spectroscopy. All measurements were performed with the samples in a cryostat in a helium atmosphere at 77 K. Continuous-wave laser diodes with emission wavelengths of 445, 650, and 808 nm and modulated at 180 Hz with a mechanical chopper were used to pump the sample. The output from a halogen lamp was passed through a monochromator and focused onto the sample to give the probe beam. A mask with a ∼1.2 mm diameter hole was used for both aligning the overlapping beams and defining the measurement area. The transmitted probe beam was guided into a second monochromator with mirrors, and the signal was measured with amplified Si (Thorlabs PDA100A) and InGaAs (Thorlabs PDA20CS) detectors. Phase-sensitive lock-in (Stanford Research System SR530 amplifier) techniques were used, with the phase set to the value that gave the maximum fluorescence signal from the sample.

■ ASSOCIATED CONTENT

Supporting Information

Current density−voltage curves; EQE, reflection, and parasitic absorption spectra; absorption onset and absorption/PL method for optical gap estimation; optical modeling for thin and thick junctions; and estimating the uncertainty of IQE evaluation. This material is available free of charge via the Internet at http://pubs.acs.org.

■ AUTHOR INFORMATION

Corresponding Authors

p.burn2@uq.edu.au
meredith@physics.uq.edu.au

Notes

The authors declare no competing financial interest.

■ ACKNOWLEDGMENTS

A.A. is funded by a University of Queensland International scholarship (UQI). I.K. is supported by a UQ Postdoctoral Research Fellowship and Australian Research Council (ARC) Centres of Excellence for Engineered Quantum Systems (CE110001013) and Quantum Computation and Communication Technology (CE110001027). P.E.S. is supported by an ARC Discovery Early Career Researcher Award (DE120101721). P.L.B. and P.M. are UQ Vice-Chancellor's Senior Research Fellows, and P.M. is an Australian Research Council Discovery Outstanding Research Award Fellow. We acknowledge funding from the University of Queensland (Strategic Initiative—Centre for Organic Photonics and Electronics), the Queensland Government (National and International Research Alliances Program), and the Australian Renewable Energy Agency (Australian Centre for Advanced Photovoltaics). This work was performed in part at the Queensland node of the Australian National Fabrication Facility, a company established under the National Collaborative Research Infrastructure Strategy to provide nano- and microfabrication facilities for Australia's researchers. We thank Pascal Wolfer for help in DPP-DTT processing conditions, Scott Watkins and the CSIRO for access to PESA measurements, and SJPC (Canada) for the high-temperature GPC analyses.

■ REFERENCES

(1) Kingsbury, E. F.; Ohl, R. S. *Bell Syst. Technol. J.* **1952**, *31*, 802.
(2) Hoppe, H.; Sariciftci, N. S. *J. Mater. Res.* **2004**, *19*, 1924.
(3) Li, G.; Zhu, R.; Yang, Y. *Nat. Photonics* **2012**, *6*, 153.
(4) Mayer, A. C.; Scully, S. R.; Hardin, B. E.; Rowell, M. W.; McGehee, M. D. *Mater. Today* **2007**, *10*, 28.
(5) Knupfer, M. *Appl. Phys. A: Mater. Sci. Process.* **2003**, *77*, 623.
(6) Jamieson, F. C.; Agostinelli, T.; Azimi, H.; Nelson, J.; Durrant, J. R. *J. Phys. Chem. Lett.* **2010**, *1*, 3306.
(7) Rao, A.; Chow, P. C.; Gélinas, S.; Schlenker, C. W.; Li, C.-Z.; Yip, H.-L.; Jen, A. K.-Y.; Ginger, D. S.; Friend, R. H. *Nature* **2013**, *500*, 435.
(8) Clarke, T. M.; Durrant, J. R. *Chem. Rev.* **2010**, *110*, 6736.
(9) Rand, B. P.; Burk, D. P.; Forrest, S. R. *Phys. Rev. B* **2007**, *75*, 115327.
(10) Scharber, M. C.; Mühlbacher, D.; Koppe, M.; Denk, P.; Waldauf, C.; Heeger, A. J.; Brabec, C. J. *Adv. Mater.* **2006**, *18*, 789.
(11) Scharber, M.; Sariciftci, N. *Prog. Polym. Sci.* **2013**, *38*, 1929.
(12) Brédas, J.-L.; Beljonne, D.; Coropceanu, V.; Cornil, J. *Chem. Rev.* **2004**, *104*, 4971.
(13) Brédas, J.-L.; Norton, J. E.; Cornil, J.; Coropceanu, V. *Acc. Chem. Res.* **2009**, *42*, 1691.
(14) Cowan, S. R.; Banerji, N.; Leong, W. L.; Heeger, A. J. *Adv. Funct. Mater.* **2012**, *22*, 1116.
(15) Bakulin, A. A.; Hummelen, J. C.; Pshenichnikov, M. S.; Van Loosdrecht, P. H. *Adv. Funct. Mater.* **2010**, *20*, 1653.
(16) Hou, J.; Chen, H.-Y.; Zhang, S.; Chen, R. I.; Yang, Y.; Wu, Y.; Li, G. *J. Am. Chem. Soc.* **2009**, *131*, 15586.
(17) Burkhard, G. F.; Hoke, E. T.; Scully, S. R.; McGehee, M. D. *Nano Lett.* **2009**, *9*, 4037.
(18) Zhang, Y.; Pandey, A. K.; Tandy, K.; Dutta, G. K.; Burn, P. L.; Meredith, P.; Namdas, E. B.; Patil, S. *Appl. Phys. Lett.* **2013**, *102*, 223302.
(19) Coffey, D. C.; Larson, B. W.; Hains, A. W.; Whitaker, J. B.; Kopidakis, N.; Boltalina, O. V.; Strauss, S. H.; Rumbles, G. *J. Phys. Chem. C* **2012**, *116*, 8916.
(20) Fang, Y.; Pandey, A. K.; Nardes, A. M.; Kopidakis, N.; Burn, P. L.; Meredith, P. *Adv. Energy Mater.* **2013**, *3*, 54.
(21) Koster, L.; Shaheen, S. E.; Hummelen, J. C. *Adv. Energy Mater.* **2012**, *2*, 1246.
(22) Bakulin, A. A.; Rao, A.; Pavelyev, V. G.; van Loosdrecht, P. H.; Pshenichnikov, M. S.; Niedzialek, D.; Cornil, J.; Beljonne, D.; Friend, R. H. *Science* **2012**, *335*, 1340.
(23) Grancini, G.; Maiuri, M.; Fazzi, D.; Petrozza, A.; Egelhaaf, H.; Brida, D.; Cerullo, G.; Lanzani, G. *Nat. Mater.* **2012**, *12*, 29.

(24) Jailaubekov, A. E.; Willard, A. P.; Tritsch, J. R.; Chan, W.-L.; Sai, N.; Gearba, R.; Kaake, L. G.; Williams, K. J.; Leung, K.; Rossky, P. J. *Nat. Mater.* **2012**, *12*, 66.
(25) Chen, K.; Barker, A. J.; Reish, M. E.; Gordon, K. C.; Hodgkiss, J. M. *J. Am. Chem. Soc.* **2013**, *135*, 18502.
(26) Armin, A.; Zhang, Y.; Burn, P. L.; Meredith, P.; Pivrikas, A. *Nat. Mater.* **2013**, *12*, 593.
(27) Scharber, M. *Nat. Mater.* **2013**, *12*, 594.
(28) Park, S. H.; Roy, A.; Beaupré, S.; Cho, S.; Coates, N.; Moon, J. S.; Moses, D.; Leclerc, M.; Lee, K.; Heeger, A. J. *Nat. Photonics* **2009**, *3*, 297.
(29) Armin, A.; Juska, G.; Ullah, M.; Velusamy, M.; Burn, P. L.; Meredith, P.; Pivrikas, A. *Adv. Energy Mater.* **2014**, *4*, 1300954.
(30) Pandey, A. K.; Aljada, M.; Pivrikas, A.; Velusamy, M.; Burn, P. L.; Meredith, P.; Namdas, E. B. *ACS Photon.* **2014**, *1*, 114.
(31) Armin, A.; Velusamy, M.; Wolfer, P.; Zhang, Y.; Burn, P. L.; Meredith, P.; Pivrikas, A. *ACS Photon.* **2014**, *1*, 173.
(32) Burkhard, G. F.; Hoke, E. T.; McGehee, M. D. *Adv. Mater.* **2010**, *22*, 3293.
(33) Dimitrov, S. D.; Bakulin, A. A.; Nielsen, C. B.; Schroeder, B. C.; Du, J.; Bronstein, H.; McCulloch, I.; Friend, R. H.; Durrant, J. R. *J. Am. Chem. Soc.* **2012**, *134*, 18189.
(34) Lee, J.; Vandewal, K.; Yost, S. R.; Bahlke, M. E.; Goris, L.; Baldo, M. A.; Manca, J. V.; Voorhis, T. V. *J. Am. Chem. Soc.* **2010**, *132*, 11878.
(35) Li, W.; Hendriks, K. H.; Roelofs, W.; Kim, Y.; Wienk, M. M.; Janssen, R. A. *Adv. Mater.* **2013**, *25*, 3182.
(36) Kim, H. J.; Lee, H. H.; Kim, J. J. *Macromol. Rapid Commun.* **2009**, *30*, 1269.
(37) Clulow, A. J.; Armin, A.; Lee, K. H.; Pandey, A. K.; Tao, C.; Velusamy, M.; James, M.; Nelson, A.; Burn, P. L.; Gentle, I. R. *Langmuir* **2014**, *30*, 1410.
(38) Lakowicz, J. R. *Principles of fluorescence spectroscopy*, 3rd ed.; Springer: New York, 2006; p 6.
(39) Yu, J.; Lee, K. H.; Zhang, Y.; Klein, M. F.; Colsmann, A.; Lemmer, U.; Burn, P. L.; Lo, S.-C.; Meredith, P. *Polym. Chem.* **2011**, *2*, 2668.
(40) Ohkita, H.; Cook, S.; Astuti, Y.; Duffy, W.; Tierney, S.; Zhang, W.; Heeny, M.; McCulloch, I.; Nelson, J.; Bradley, D. D. C.; Durrant, J. R. *J. Am. Chem. Soc.* **2008**, *130*, 3030.
(41) Mescher, J.; Christ, N.; Kettlitz, S.; Colsmann, A.; Lemmer, U. *Appl. Phys. Lett.* **2012**, *101*, No. 073301.
(42) Xu, H.; Jiang, Y.; Li, J.; Ong, B. S.; Shuai, Z.; Xu, J.; Zhao, N. *J. Phys. Chem. C* **2013**, *117*, 6835.
(43) Coffin, R. C.; Peet, J.; Rogers, J.; Bazan, G. C. *Nat. Chem.* **2009**, *1*, 657.
(44) Li, J.; Zhao, Y.; Tan, H. S.; Guo, Y.; Di, C.-A.; Yu, G.; Liu, Y.; Lin, M.; Lim, S. H.; Zhou, Y. *Sci. Rep.* **2012**, *2*, 754.
(45) Pettersson, L. A.; Roman, L. S.; Inganäs, O. *J. Appl. Pys.* **1999**, *86*, 487.